JOURNAL OF
biomaterials
applications

Biomaterials Processing

Journal of Biomaterials Applications
2020, Vol. 34(8) 1114–1130

DOI: 10.1177/0885328219898385
journals.sagepub.com/home/jba
SAGE

Hybrid manufacturing strategies for tissue engineering scaffolds using methacrylate functionalised poly(glycerol sebacate)

Samand Pashneh-Tala, Robert Moorehead and Frederik Claeyssens

Abstract

Poly(glycerol sebacate) is an attractive biomaterial for tissue engineering due to its biocompatibility, elasticity and rapid degradation rate. However, poly(glycerol sebacate) requires harsh processing conditions, involving high temperatures and vacuum for extended periods, to produce an insoluble polymer matrix. These conditions make generating accurate and intricate geometries from poly(glycerol sebacate), such as those required for tissue engineering scaffolds, difficult. Functionalising poly(glycerol sebacate) with methacrylate groups produces a photocurable polymer, poly(glycerol sebacate)-methacrylate, which can be rapidly crosslinked into an insoluble matrix. Capitalising on these improved processing capabilities, here, we present a variety of approaches for fabricating porous tissue engineering scaffolds from poly(glycerol sebacate)-methacrylate using sucrose porogen leaching combined with other manufacturing methods. Mould-based techniques were used to produce porous disk-shaped and tubular scaffolds. Porogen size was shown to influence scaffold porosity and mechanical performance, and the porous poly(glycerol sebacate)-methacrylate scaffolds supported the proliferation of primary fibroblasts in vitro. Additionally, scaffolds with spatially variable mechanical properties were generated by combining variants of poly(glycerol sebacate)-methacrylate with different stiffness. Finally, subtractive and additive manufacturing methods were developed with the capabilities to generate porous poly (glycerol sebacate)-methacrylate scaffolds from digital designs. These hybrid manufacturing strategies offer the ability to produce accurate macroscale poly(glycerol sebacate)-methacrylate scaffolds with tailored microscale porosity and spatially resolved mechanical properties suitable for a broad range of applications across tissue engineering.

Keywords

Tissue engineering, photocurable, porogen, 3D cell culture, subtractive manufacturing, 3D printing, additive manufacturing

Introduction

Tissue engineering aims to produce functional replacement tissues and organs for the treatment of injury or disease.[1] A common strategy in tissue engineering is the use of degradable synthetic polymer scaffolds, which provide a base for cell attachment and tissue growth.[2] These scaffolds act as a substitute extracellular matrix (ECM), providing mechanical support and guidance for infiltrating cells, and also as a template, directing the shape of the final tissue construct.

Poly(glycerol sebacate) (PGS) is an attractive synthetic polymer for producing tissue engineering scaffolds.[3] This biocompatible, elastomeric and degradable polyester has been employed in heart,[4–6] vascular,[7–9] retinal,[10] nerve[11] and cartilage[12–14] tissue engineering, as a polymer scaffold or support structure. PGS is simple to synthesise as a soluble prepolymer using the relatively inexpensive and naturally occurring monomers glycerol (a basic building block of lipids) and sebacic acid (an intermediate in the metabolism of medium- to long-chain fatty acids).[15] However, to form PGS from its

Kroto Research Institute, The University of Sheffield, Sheffield, UK

Corresponding author:
Samand Pashneh-Tala, Kroto Research Institute, The University of Sheffield, Broad Lane, Sheffield S3 7HQ, UK.
Email: s.pashneh-tala@sheffield.ac.uk

prepolymer components, it must be thermally cured to form an insoluble matrix. This requires a combination of high temperatures and vacuum for extended periods of time, and these processing conditions impose significant difficulties on the production of intricate and precise shapes.[15,16]

Both microscale and macroscale architecture is important in tissue engineering scaffold design. These scaffolds often require high porosities, with minimum feature sizes on the order of micrometres, to fulfil their functions as ECM substitutes by facilitating cell infiltration, mass transport and nutrient exchange.[17–20] On the macroscale, the scaffolds must also be able to reproduce the shapes of the human body's tissues and organs, and this may be required in a user-defined manner given the highly personalised nature of many tissue engineering applications.[1,21] The requirement for thermal curing of PGS therefore restricts design freedom and limits the applications of the polymer as a tissue engineering scaffold material due to its shortcomings in shape formation.

To counter this, PGS prepolymer may be functionalised to render it photocurable. In combination with a free radical generating photoinitiator and an appropriate wavelength of light, the functionalised PGS prepolymer rapidly crosslinks into an insoluble matrix at room temperature and pressure.[22–25] We recently reported on the synthesis of a methacrylate functionalised PGS (PGS-M) and demonstrated its excellent biocompatibility and tunable properties.[26] By altering the degree of methacrylation (DM) of PGS-M, it was possible to modulate the material's mechanical properties and degradation rate; a valuable attribute, given the effects these properties have on cell behaviour and ECM deposition in tissue engineering scaffolds.[8,27–31] We were also able to fabricate microscale scaffold structures from PGS-M using 2-photon polymerisation (2PP). These scaffolds displayed minimum feature sizes of $\sim$10 μm and supported cell proliferation. However, the relatively labour-intensive and time-consuming 2PP process limits its utility to generating only small scaffolds (micrometre–millimetre scale) with limited use given the length scales usually required for tissue engineering applications (millimetre–centimetre).

Here, we describe alternative manufacturing strategies for producing tissue engineering scaffolds from PGS-M, at useful length scales, using porogen leaching combined with a variety of other methods. Porogen leaching is a simple approach for generating porous polymer structures. The polymer material, either liquid or solvated, is combined with porogen particles to form a mixture. The polymer then solidifies, through cooling, chemical crosslinking or solvent removal, producing a composite. The porogens are then removed by dissolution in a solvent in which the polymer is insoluble, yielding a porous structure.

Porogen leaching is one of the earliest established methods for producing porous polymer scaffolds for tissue engineering. The process is simple and does not require specialised equipment. Porogen leaching has been utilised with a wide variety of materials to generate scaffolds for various tissue engineering applications, including bone,[32–34] cardiac tissue,[35] blood vessels,[7,9,36,37] muscle,[38] cartilage[39–42] and skin.[43] Controlling porogen volume, size and shape offer simple ways to alter the porosity and pore architecture of the resulting scaffolds, allowing tailoring of the microstructure towards specific cell types and applications.[9,19,41,44–47] Achieving macroscale geometric accuracy and suitable mechanical properties within scaffolds produced using porogen leaching can be challenging. This is often a result of the loss of solvents, used to dissolve the scaffold material to allow mixing with the porogens, leading to shrinking or cracking.[48–51]

Using mould-based techniques, and subtractive and additive manufacturing, we have developed various hybrid strategies for producing millimetre–centimeter scale tissue engineering scaffolds using PGS-M combined with sucrose porogens. Sucrose is inherently biocompatible and can be easily obtained in fractions of various sizes. Using sucrose particles of different sizes, highly porous PGS-M scaffolds with tunable microstructures were generated. Our methods did not require solvents which resulted in reduced scaffold shrinkage and cracking, improving accuracy and quality. The porous PGS-M scaffolds were shown to support cell proliferation and ingrowth during in vitro culture. Moulding techniques were used to fabricate disk-shaped and tubular scaffolds with open surface porosities. Moulding also permitted the valuable combination of variants of PGS-M with different stiffness into a single scaffold, offering interesting potential applications in tissue environments with transitional mechanical properties, such as cartilage-to-bone,[52] tendons (muscle-to-bone) and ligaments (bone-to-bone).[53] Finally, using subtractive and additive manufacturing allowed the realisation of intricate scaffolds with inherent porosity from digital designs, enabling personalised or customised solutions.

The presented approaches provide the ability to generate a variety of accurate macroscale PGS-M scaffold designs with tailored microscale porosity and spatially variable mechanical properties. These methods allow the favourable material properties of PGS-M as a biomaterial to be exploited, offering potential applications across the tissue engineering field.

Materials and methods

In the following methods, all chemical reagents were obtained from Merck, UK unless otherwise stated.

Synthesis of PGS-M prepolymer

PGS-M was synthesised as described previously.[26] Briefly, PGS prepolymer was formed from equimolar amounts of sebacic acid and glycerol (Fisher Scientific, UK) combined at 120°C, under nitrogen gas for 24 h, followed by the application of a vacuum for a further 24 h. The secondary hydroxyl groups of the glycerol subunits within the PGS prepolymer were then functionalised with methacrylate groups to yield photocurable PGS-M prepolymer. About 3.9 mmol of hydroxyl groups per gram of PGS prepolymer were assumed available for methacrylation, based on both of the primary hydroxyl groups present in the glycerol having reacted with sebacic acid. PGS prepolymer was dissolved in dichloromethane (Fisher Scientific, UK) 1:4 (w/v) and equimolar methacrylic anhydride and triethylamine, slowly added. Three different concentrations of methacrylic anhydride were used (0.3, 0.5 and 0.8 mol/mol of PGS prepolymer hydroxyl groups) to vary the DM of the resulting PGS-M from 30 to 50 to 80%, respectively. 4-Methoxyphenol was also added at 1 mg/g of PGS prepolymer. The reaction was performed at 0°C and allowed to rise to room temperature over 24 h. The solution was then washed with 30 mM hydrochloric acid (Fisher scientific, UK) at 1:1 (v/v) and dried with calcium chloride (Fisher scientific, UK), and the dichloromethane was removed via rotary evaporation, under vacuum.

Fabrication of porous disk-shaped PGS-M scaffolds using porogen leaching

PGS-M prepolymer with 30% DM was combined 1% (w/w) with the photoinitiator diphenyl(2,4,6-trimethylbenzoyl) phosphine oxide/2-hydroxy-2-methylpropiophenone (50/50 blend) (further denoted as photoinitiator) and then mixed thoroughly with sucrose particles (Tate & Lyle, UK). The sucrose particles were prepared in four different size ranges using mechanical sieving (Endecotts Minor 200 with square grid sieves, UK): 100–200 μm, 50–100 μm, 38–50 μm, and a 1:1 blend of 50–100 μm:38–50 μm (further denoted as large, medium, small and mixed, respectively). The PGS-M and sucrose mixtures were packed into silicone moulds (7.3 mm diameter, 2 mm deep) and then photocured under UV light (100 W, OmniCure Series 1000 curing lamp) for 5 min on each side. The resulting PGS-M and sucrose composite disks were then washed in dH_2O for four days to dissolve the sucrose particles; then methanol for four-days to remove any soluble PGS-M prepolymer and residual photoinitiator and finally in dH_2O again, yielding porous PGS-M scaffolds. Washes of dH_2O and methanol were refreshed daily.

The sucrose particles and PGS-M prepolymer were mixed at different ratios (w/w) depending on the particle size range used. Optimum ratios (sucrose particles: PGS-M) were selected based on the handling characteristics and integrity of the resulting scaffolds. For the large, medium, mixed and small sucrose particles, the optimum ratios were determined to be 2.8:1, 3:1, 3.8:1 and 3.4:1, respectively.

Scanning electron microscopy of porous PGS-M scaffolds

Porous disk-shaped PGS-M scaffolds produced from the optimum ratios of PGS-M to sucrose particles were examined using scanning electron microscopy (SEM). Four-millimetre diameter disks were cut from wet scaffolds using a dissection punch and freeze-dried for 24 h. The dry scaffolds were gold coated (Edwards S150B sputter coater) and examined using SEM (Philips XL-20) at 13–15 kV.

Pore sizes were semi-quantitatively assessed using the SEM images and image analysis software (ImageJ, version 1.45 s). Sixty pores were randomly selected from each image, using an overlaid grid of crosses, and their areas measured using the freehand selection tool. Measurements were calibrated using the image scale bars. The mean average pore areas for each scaffold type, calculated from the image analysis, were then multiplied by a statistical correction factor of $2/(3_{1/2})$ (pores assumed to be spherical) to adjust for the arbitrary, non-equatorial location of the section through each pore.[54] This generated the average pore area, in the equatorial plane, for each scaffold type examined. Additionally, the average pore diameter was also calculated, after the application of the correction factor. Three SEM images from triplicate scaffold samples were examined.

PGS-M scaffold porosity quantification using helium pycnometry

The porosity of the disk-shaped PGS-M scaffolds produced using the different sucrose particle sizes was determined using helium pycnometry (AccuPyc 1340, Micromeritics, USA) ($N = 3$, $n = 3$). Four-millimetre diameter disks were cut from wet scaffolds and freeze-dried. The diameters and thickness of the dry scaffolds were measured using digital callipers. This determined the macroscopic volume of the scaffolds, ignoring the porosity. The scaffolds were then placed in the pycnometer using a 0.1-cm^3 chamber insert. The chamber was pressurised with helium at 19,500 psi, and the volume occupied by the scaffolds was determined. This was the true volume of the

scaffolds, including the porosity. The scaffold porosity was then calculated using the following equation

$$\left(1 - \frac{\text{true volume}}{\text{macroscopic volume}}\right) \times 100 = \text{porosity } (\%)$$

Characterisation of porous PGS-M scaffolds by Raman spectroscopy

Disk-shaped 30% DM PGS-M scaffolds (7.3 mm diameter, 2 mm thick) produced using mixed sucrose particles at the optimum sucrose particle to PGS-M ratio were fabricated and freeze-dried, as described above. These scaffolds were referred to as leached. Additional scaffolds were also produced, in a similar manner, but without being washed in dH_2O or methanol following photocuring to allow complete retention of the sucrose. These scaffolds were referred to as non-leached. The leached and non-leached scaffolds were cut diametrically, and their interiors were analysed by Raman spectroscopy (Thermo Scientific Nicolet DXR) using a 10 mW, 532 nm laser at 2 cm^{-1} resolution, between Raman shifts of 4000 cm^{-1} and 400 cm^{-1}. The exposure time was 10 s, with 20 exposures taken per sample, and the spectrograph aperture set at 50 μm. Fluorescence correction was also applied. In addition to the scaffolds, mixed sucrose particles alone, a flat non-porous disk of photocured 30% DM PGS-M and a sample of 30% DM PGS-M prepolymer were also examined, as material controls.

Culture of fibroblasts on porous PGS-M scaffolds

Porous disk-shaped PGS-M scaffolds (7.3 mm diameter, 2 mm thick) were produced in silicone moulds, as described above, using medium sucrose particles at the optimum sucrose particle to PGS-M ratio (3:1). Following leaching of sucrose particles, the scaffolds were sterilised by autoclave at 121°C for 30 min. The sterile scaffolds were placed individually in the wells of 96-well tissue culture plates (Greiner bio-one, Germany), and 200 μl of foetal calf serum (FCS) was added to each well. The scaffolds were placed in an incubator at 37°C and 5% CO_2, for 24 h. The FCS was then removed, and the scaffolds were rinsed thrice with PBS, in preparation for cell seeding.

Human dermal fibroblasts from primary dermal tissue were obtained with informed consent (ethics reference: 15/YH/0177) and processed and stored in accordance with the Human Tissue Act 2004 (licence number 12179). Fibroblasts were cultured to between passages 7 and 8 in growth medium composed of Dulbecco's modified Eagle's medium AQmedia modified with 10% (v/v) FCS, 1% (v/v) penicillin (10,000 U/ml), 1% (v/v) streptomycin (10 mg/ml) and 0.25% (v/v) amphotericin B (250 μg/ml). Fibroblasts were harvested using trypsin (0.025%)/EDTA (0.01%) solution and resuspended in growth medium at 320×10^3 cells/ml. Two hundred microliters of cell suspension were applied to each scaffold (equivalent to 64,000 cells per scaffold, 200,000 cells/cm^2 of scaffold surface). The seeded scaffolds were returned to the incubator for 6 h to allow for cell attachment, and then the growth medium was replaced. The scaffolds were cultured for a further 18 h (producing a culture period of one day post seeding) or seven days. Unseeded scaffolds were also incubated, in parallel with the seeded scaffolds, as negative controls. The growth medium was replaced every other day.

The quantity of cells present on the cultured scaffolds ($N = 3$, $n = 3$ for each time point) was assessed using the PicoGreen® DNA quantification assay, purchased as a kit (Thermo Fisher Scientific, USA). At the conclusion of the cell culture, the scaffolds were washed thrice with PBS and then frozen and thawed thrice in 500 μl of dH_2O. The solutions from each well were agitated in a vortex mixer and then centrifuged at 7000 g for 5 min (Sanyo MSE Micro Centaur MSB010. CX2.5). One hundred and eighty microlitres of the supernatants were then mixed with 180 μl of a 5% (v/v) TE buffer and 0.5% (v/v) PicoGreen® solution in dH_2O for 10 min, in the absence of light. One hundred microlitres, in triplicate, were then extracted from each solution, placed in black 96-well plates and read using a fluorescence plate reader (Bio-tek instruments FLX800) at 480 nm excitation and 520 nm emission. The reading from a blank composed of dH_2O mixed with the TE buffer and PicoGreen® solution was then subtracted from the value for each well. Fluorescence values were converted into mass of DNA using a standard curve generated from analysing λ DNA at 200, 400, 600, 800 and 1000 ng/ml, supplied with the assay kit.

Additionally, the cultured scaffolds were also examined using histology. At the conclusion of the culture periods, the seeded scaffolds and unseeded controls were washed thrice with PBS and then fixed with 3.7% formaldehyde. The fixed scaffolds were then frozen in OCT compound (Tissue-Tek, Sakura, Japan) and cut into 5 μm sections at –20°C before being mounted on glass slides and stained with haematoxylin and eosin (H&E). Stained sections were imaged using light microscopy (Motic B5 professional series).

Manufacture of porous tubular PGS-M scaffolds

Porous tubular PGS-M scaffolds were produced using mixed sucrose particles combined 3.8:1 (w/w) with 30% DM PGS-M prepolymer and photoinitiator, as described above. One-millilitre polypropylene syringes

(Terumo), modified by removing their ends, were used as moulds. Five different manufacturing methods were explored (see Supplemental material) with only the most successful method described here. A syringe mould was filled with PGS-M and sucrose mixture and a 3 mm diameter core then cut out of the mixture, using a stainless steel die. The core space was then filled with sucrose particles, and the construct was extruded from the mould and then photocured. Following photocuring, the construct was washed in dH_2O and methanol, as described above, to remove the sucrose, soluble PGS-M prepolymer and photoinitiator. The resulting porous tubular scaffolds were bisected along their length, freeze-dried and imaged using SEM, as described above, to examine their structure.

Manufacture of porous, multi-stiffness, PGS-M scaffolds

Porous PGS-M scaffolds were produced with spatially variable mechanical properties. Medium sucrose particles were mixed with PGS-M prepolymers of 30, 50 and 80% DM at a ratio of 3:1 (w/w) and with photoinitiator, as described above. These mixtures were packed into a rectangular silicone mould ($40 \times 10 \times 2$ mm), in equal quantities, such that the DM of the PGS-M prepolymer varied long its length, from 30 to 50 to 80%. The PGS-M and sucrose mixtures were then photocured for 5 min on each side, as described above. The resulting rectangular structure was then washed four times in dH_2O to dissolve the included sucrose particles, followed by washes in methanol and dH_2O, as described above. To examine their mechanical behaviour, the multi-stiffness scaffolds were secured in grips and subjected to tensile loading (Hounsfield H100KS) at a crosshead speed of 50 mm/min with samples elongated to failure ($n = 3$). Additionally, to examine their internal structure, the multi-stiffness scaffolds were cut along their length, freeze-dried and imaged using SEM, as described above.

Subtractive manufacturing of porous PGS-M scaffolds

Porous PGS-M scaffolds with complex 3 D geometry were produced using a subtractive manufacturing approach. Mixed sucrose particles were combined 3.8:1 (w/w) with 80% DM PGS-M and with photoinitiator, as described above. The mixture was formed into a flat disk, 50 mm in diameter and 10 mm thick. This disk was held within an acrylic supporting disk of equal thickness and 100 mm diameter and photocured for 5 min on each side, as described above. Following photocuring, the acrylic disk, with integrated PGS-M and sucrose disk, was mounted in a five-axis dental CNC milling machine (Roland DWX-50). Using CAD/CAM software (Solidworks 2016 SP4.0/Roland Sum 3D 2013 Rev.2), the macroscopic geometry of the scaffolds was designed virtually and machined from the photocured PGS-M and sucrose composite. A molar crown and an orbital floor plate were produced, as proof-of-concept scaffold designs. Cylindrical ball burs were used with 2, 1 and 0.6 mm diameters, rotating clockwise at 15,000, 26,000 and 27,000 r/min, with 1400, 800 and 400 *XYZ* feed rates, respectively. No coolant was used. Following machining, the scaffolds were removed from the surrounding PGS-M and sucrose composite. The diameters of the holes of the orbital floor plate were measured using digital callipers ($n = 6$) to determine the accuracy of the machining process. The scaffolds were then placed in four washes of dH_2O to dissolve the included sucrose particles. The resulting porous scaffold structures were then washed in methanol and dH_2O, as described above. To examine the structure of the scaffolds, they were freeze-dried and imaged using SEM, as described above.

Additive manufacturing of porous PGS-M scaffolds

Proof-of-concept PGS-M scaffolds were produced using a modified additive manufacturing approach (Figure 1). Given that the PGS-M and sucrose mixture was highly viscous, we designed a materials feed system similar to selective laser sintering, while providing illumination using a UV lamp. A build chamber was constructed from a 50 ml polypropylene syringe with the end removed. With the syringe plunger positioned 3 mm from the open end, the build chamber was filled with a mixture of large sucrose particles and 30% DM PGS-M prepolymer at the optimum ratio previously determined (2.8:1), along with photoinitiator, as described above. The build chamber was then covered with a cap containing an 8 mm diameter aperture, offset 4 mm from the cap's centre. This cap ensured that only a selected region of the PGS-M and sucrose mixture was photocured. The capped build chamber was then exposed to UV light, as previously described, for 30 s. Following selective photocuring, the cap was removed and the syringe plunger retracted 1 mm. An additional layer of PGS-M and sucrose mixture was then added to the build chamber. The cap was reapplied with the aperture position rotated 10° clockwise from previous and the build chamber again exposed to UV light. Layers of PGS-M and sucrose mixture were added and selectively photocured until the cap had been rotated 360°. The contents of the syringe build chamber were then extruded into methanol, dissolving the PGS-M prepolymer that had not been photocured, leaving behind the selectively photocured PGS-M with included sucrose particles as

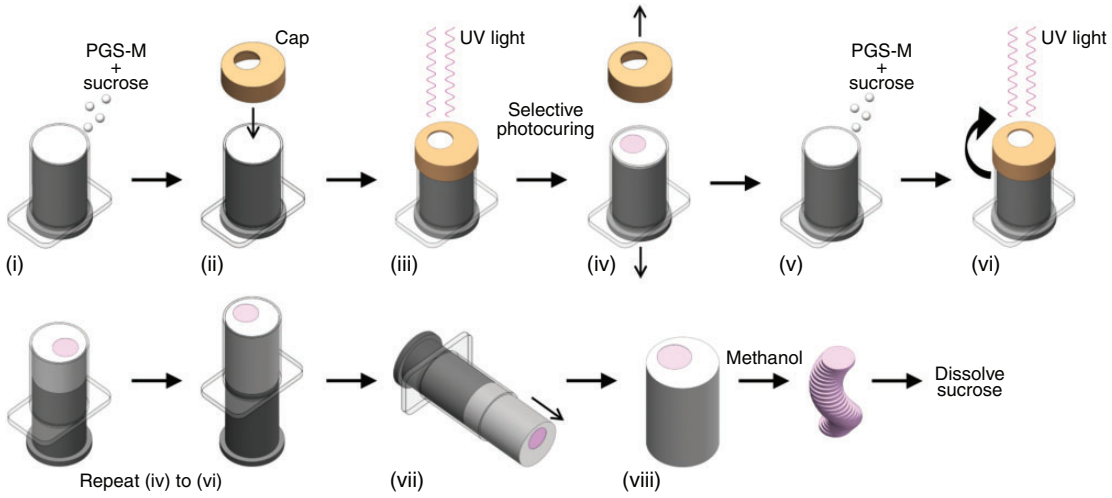

Figure 1. Additive manufacturing of porous PGS-M scaffolds: (i) build chamber set at 3 mm deep and filled with PGS-M and sucrose mixture; (ii) cap placed over build chamber for selective photocuring; (iii) PGS-M selectively photocured through the cap aperture; (iv) cap removed and build chamber retracted 1 mm; (v) additional PGS-M and sucrose mixture added to the build chamber; (vi) cap replaced, rotated 10° clockwise from the previous position, and PGS-M selectively photocured again. Steps (iv) to (vi) were repeated until the cap had completed a full 360° revolution; (vii) PGS-M and sucrose mixture extruded from the build chamber; (viii) PGS-M and sucrose mixture washed in methanol to reveal the selectively photocured PGS-M construct with included sucrose particles. The sucrose particles were then leached in dH_2O.

a 3D-printed spiral construct (see Supplemental video). The sucrose particles were removed from the construct by washing in dH_2O, and the resulting porous scaffold structure was washed in methanol and dH_2O, as described above. To examine their internal structure, the 3D-printed scaffolds were cut in half, freeze-dried and imaged using SEM, as described above.

Statistical analysis

Scaffold pore area and porosity results were statistically analysed using one-way ANOVA with Tukey's multiple comparison analysis. PicoGreen® DNA quantification assay results following fibroblast cultures were statistically analysed using two-way ANOVA with Tukey's multiple comparison analysis. $P < 0.05$ was considered significant in all analyses. All error bars presented represent standard deviation.

Results and discussion

Characterisation of porous PGS-M scaffolds produced by porogen leaching

Porous scaffolds for tissue engineering were produced from PGS-M using porogen leaching. PGS-M prepolymer was combined with sucrose particles and photocured forming a composite. The sucrose was then dissolved to produce porous scaffold structures.

Sucrose particles of different size ranges were used. For each size range, the optimum ratio of sucrose particles to PGS-M prepolymer was determined based on maximising sucrose content, which would ultimately generate the scaffold's porosity, while maintaining suitable scaffold handling characteristics. The optimum ratios of sucrose particles to PGS-M determined were 2.8:1, 3:1, 3.8:1 and 3.4:1 for the disk-shaped scaffolds produced from the large, medium, mixed and small sucrose particle sizes, respectively. The highest ratio of sucrose particles to PGS-M was achieved using the mixed size range, which contained both medium and small particles. This mixture of particle sizes likely permitted more efficient packing within the moulds during fabrication. SEM revealed the sizes of the pores present in the scaffolds appeared to correlate with the different sizes of sucrose porogen particles used to produce them (Figure 2(a)). Average pore size was calculated as equatorial area and diameter (Figure 2(b) and (c)) with the assumption the pores were spherical. The sizes of the pores produced by the different sizes of sucrose particles were significantly different ($P < 0.05$). The effect of porogen particle size on scaffold pore size has been well established when using porogen leaching.[9,19,49,55,56] Given that scaffold pores can affect cell phenotype and proliferation, achieving pore size modulation by the simple selection of different-sized porogen particles is a key advantage of the porogen leaching process.[19,46,47] Interconnectivity between pores was also visible in all scaffolds.

Helium pycnometry determined that the scaffolds produced using the mixed sucrose particles possessed the greatest porosity at $82.9 \pm 0.7\%$ (Figure 2(d)).

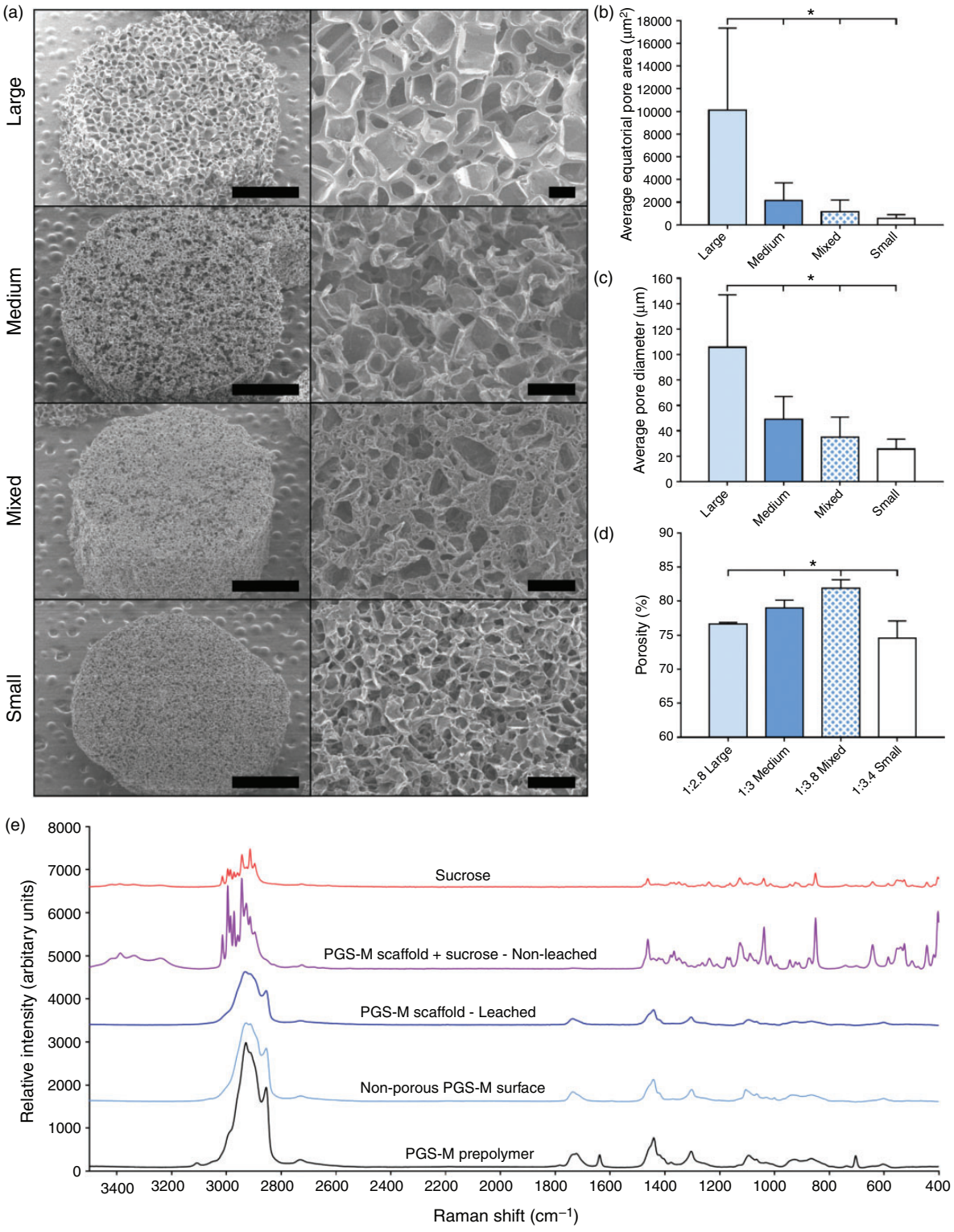

Figure 2. Pore size and porosity analysis of disk-shaped PGS-M scaffolds produced using large, medium, mixed, and small sucrose particle size ranges: (a) SEM revealed a correlation between sucrose particle size and the resulting scaffold pores. Scale bars in the left and right micrographs are 1 mm and 100 μm, respectively. Pore sizes were calculated as equatorial area (b) and diameter (c); (d) helium pycnometry showed the total porosity of the scaffolds varied with sucrose particle size; (e) Raman spectra for disk-shaped PGS-M scaffolds with sucrose included (PGS-M scaffold + sucrose – non-leached) and leached out in dH_2O (PGS-M scaffold – leached). Spectra for the PGS-M prepolymer, a non-porous PGS-M sample, and sucrose are included for comparison.

This was significantly different to the porosities of all of the other scaffolds examined ($P < 0.01$). The porosities of all of the PGS-M scaffolds produced were within the ranges of those shown to be successful for tissue engineering applications where porogen leaching was employed. These appear to range from 60 to 97%.[9,17–19] Maximising scaffold porosity is advantageous for tissue engineering. Greater porosity assists cell ingrowth, mass transport and nutrient exchange and, in the case of degradable scaffold materials, facilitates increased degradation rates.[17–20]

It was noted that the porous PGS-M scaffolds did not display any cracking or voids following photocuring, leaching or freeze-drying. These are common problems associated with using solvents in the manufacture of porous polymer scaffolds through porogen leaching.[48–51] These findings therefore demonstrate an advantage of utilising a photocurable liquid prepolymer, such as PGS-M, in porogen leaching. A small amount of shrinkage was observed within the PGS-M scaffolds during fabrication. However, this was largely associated with the freeze-drying process (see Supplemental material). No significant difference was seen between the dimensions of the scaffolds following photocuring and porogen leaching.

The PGS-M polymer and scaffolds were examined using Raman spectroscopy (Figure 2(e)). The major peaks present in the spectra from the PGS-M prepolymer, non-porous PGS-M sample and leached PGS-M scaffold at 1100, 1450 and 2900 cm^{-1} were associated with stretching of the $C–H_2$ bonds present in the backbone of the sebacic acid.[57] Peaks at 1730 cm^{-1} were associated with the carboxylic acid end groups of the sebacic acid. The spectrum from the PGS-M prepolymer, prior to photocuring, shows a peak at 1650 cm^{-1} and a shoulder at 3000 cm^{-1}. These features are absent from the spectrum from the non-porous PGS-M sample and the PGS-M scaffold following sucrose leaching. This is expected given that these spectral features are associated with C=C bond stretching, and the PGS-M prepolymer contains methacrylate groups which are lost during photopolymerisation through opening of the C=C bond.[57] Other methacrylated polymers have shown similar results, with spectral peaks associated with the methacrylate groups disappearing after polymerisation.[58] An anomalous peak at 700 cm^{-1} is present in the PGS-M prepolymer spectra. This is associated with C–Cl bond stretching and is likely the result of residual DCM present in the prepolymer sample following synthesis. Examination of the scaffold interiors suggested that the sucrose particles had been effectively removed during the leaching process in dH_2O. The spectrum from the porous PGS-M scaffolds (leached) lacked the characteristic peaks associated with sucrose and compared well with a sample of non-porous, photocured PGS-M.

Previously, an alternative form of photocurable PGS, PGS-isocyanatoethyl methacrylate (PGS-IM), was combined with porogen leaching to generate porous scaffold structures.[22] NaCl porogens of 150–300 μm were used to generate the pores. The resulting structures showed some similarities to those described herein, although the ratio of NaCl to PGS-IM was not reported, and solvents were required to combine the polymer and porogens together. A direct comparison between the PGS-M and PGS-IM scaffolds is therefore limited. The PGS-IM scaffolds appeared to display reduced surface porosities compared to the PGS-M scaffolds and also featured large voids, possibly a result of solvent evaporation during fabrication. Based on this evidence, it would appear that the system of combining PGS-M with sucrose porogens is superior to the previously presented combination of PGS-IM with NaCl porogens.

Cell proliferation on porous PGS-M scaffolds

Fibroblasts were seeded onto porous PGS-M scaffolds to examine their biocompatibility. Quantification of dsDNA revealed that the DNA content of the scaffolds increased significantly in culture ($P < 0.001$) from day 1 to day 7 (Figure 3(a)). This suggests that the fibroblasts remained viable and were able to proliferate on the scaffolds over the culture period. Based on a single cell containing 3.5 pg of dsDNA, the number of cells present on the scaffolds increased from 67,200 ± 19,000 cells at day 1 to 211,000 ± 11,400 cells by day 7.[59] PGS-M has been shown to support the successful growth and proliferation of various primary cell types in vitro, in the form of flat surfaces and 3D-printed scaffolds manufactured by 2PP.[26] Histology staining of sections taken through the scaffolds revealed a layer of cells at the seeded surface along with cell penetration into the scaffold interiors after seven days (Figure 3(b) and (c)). Thermally cured PGS scaffolds fabricated by porogen leaching with NaCl showed similar results when seeded with fibroblasts and cultured for eight days.[60]

The results suggest that the porous PGS-M scaffolds, produced using porogen leaching, are suitable for use as tissue engineering scaffolds; supporting cell growth, proliferation and infiltration. Cell infiltration into porous tissue engineering scaffolds is key to the formation and function of the resulting tissue construct. Cell infiltration into the PGS-M scaffolds could be further enhanced by modifying the scaffold's surface chemistry;[61] utilising growth factors or chemoattractants;[33,34,62] increasing the scaffold's surface area

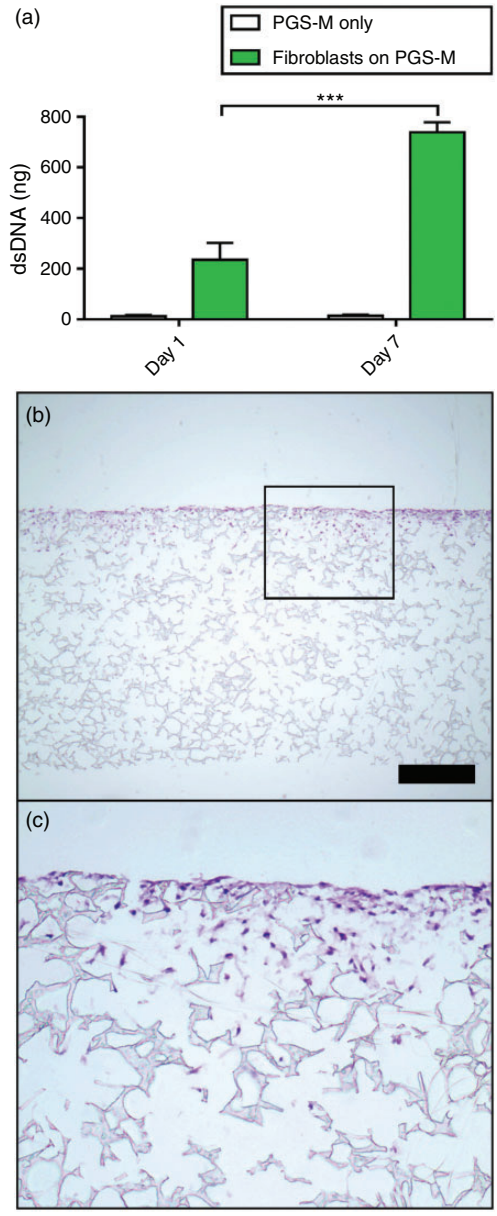

Figure 3. Fibroblast culture on porous PGS-M scaffolds: (a) a significant increase in dsDNA content was seen between day 1 and day 7 of culture ($P < 0.001$), suggesting fibroblast proliferation. Negative controls were unseeded PGS-M scaffolds (PGS-M only); (b) H&E-stained sections of PGS-M scaffolds seeded with fibroblasts after 7 days in culture. Cells were visible across the scaffold surface. The highlighted section is magnified in (c) and shows cell infiltration into the scaffold. Scale bar is 500 μm.

or interconnectivity[17,60] and applying pressure or flow-based seeding methods.[60,63,64]

Hybrid manufacturing strategies for porous PGS-M scaffolds

A number of different manufacturing methods for producing porous tissue engineering scaffolds were explored to demonstrate the versatility of using PGS-M combined with porogen leaching.

Tubular scaffolds

Tubular PGS-M scaffolds were produced using a combination of moulds, cutting dies and mechanical support (Figure 4(a)). SEM showed that the outer and luminal surfaces of the tubular scaffolds were porous, along with their interiors (Figure 4(b)). From a variety of methods explored, only this combination of processes was able to produce intact tubular scaffolds with this degree of porosity (see Supplemental material). As discussed previously, maximising scaffold porosity is advantageous in tissue engineering applications. Polymer scaffolds can be limited by reduced porosity resulting from the formation of a polymer 'skin' across their surfaces.[19] This is usually attributed to solvation of the polymer material during scaffold manufacture. Here, it has been demonstrated that using a photocurable liquid prepolymer during scaffold fabrication combined with appropriate manufacturing methods permits the production of scaffolds with open surface porosity.

The ability to generate tubular PGS-M scaffolds with porous interiors and outer and luminal surfaces may be useful in various soft tissue engineering applications, such as blood vessels,[65] oesophagus[66] or trachea.[67]

Porous, multi-stiffness, PGS-M scaffolds

PGS-M prepolymers of different DM (30, 50 and 80%) were combined with sucrose particles and formed into a single rectangular scaffold with regions of different mechanical properties along its length (Figure 5(a)). Bonding between the different regions of the scaffold appeared complete, although the region containing the 30% DM PGS-M appeared to shrink following freeze-drying, as was previously observed in the disk-shaped scaffolds. The scaffolds were subjected to tensile loading. The stress–strain response is shown in Figure 5(b). Observing the multi-stiffness scaffolds under tension revealed the different mechanical properties of the three regions. At a tensile force of 0.8 N (just prior to failure), the 30% DM region showed the greatest strain (~0.6), while the 80% DM region showed the least (Figure 5(c) and (d)). SEM revealed good interconnection between the different regions of porous PGS-M polymer (Figure 5(e)). Similar results have been observed in the production of PCL scaffolds with layers of different-sized pores produced using different-sized NaCl porogen particles.[68] These scaffolds were produced by compression-moulding and showed good interconnectivity between their different layers.

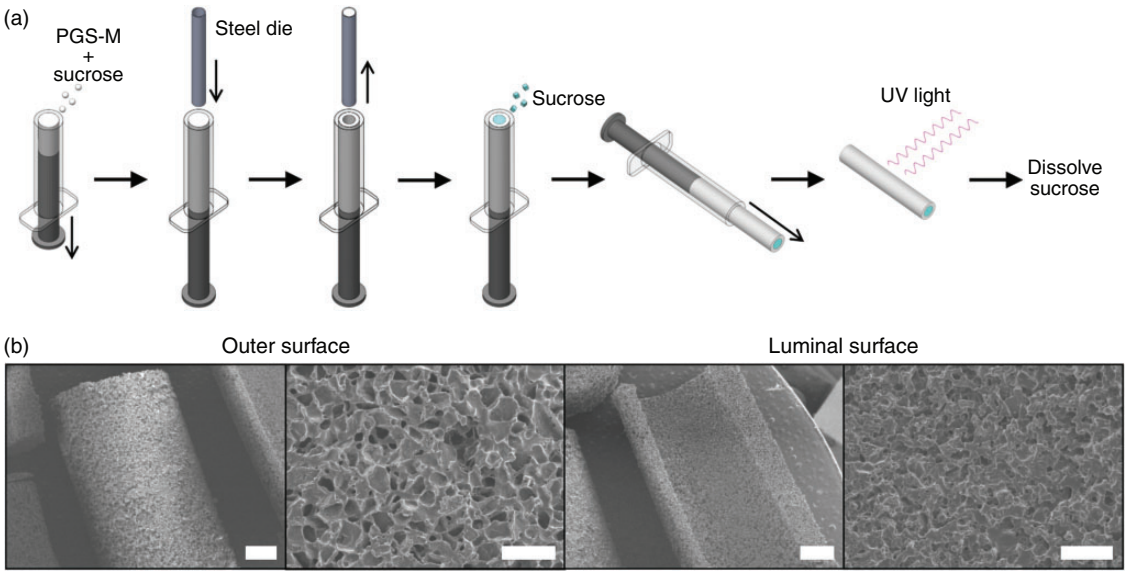

Figure 4. (a) Manufacturing process for producing porous tubular scaffolds from PGS-M combined with sucrose porogens. (b) SEM of porous tubular PGS-M scaffolds. The scaffolds displayed porous interiors along with outer and luminal surfaces. Scale bars for the lower and higher magnification images are 1 mm and 200 μm, respectively.

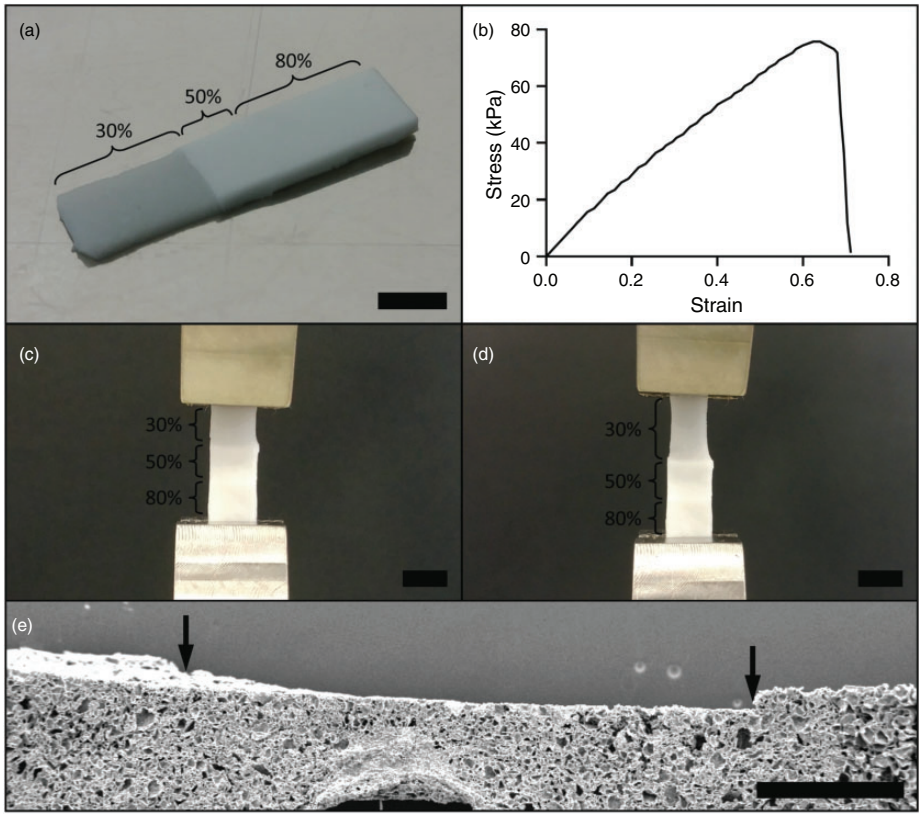

Figure 5. Porous, multi-stiffness, scaffolds composed of 30, 50 and 80% DM PGS-M: (a) the different PGS M variants were formed into single rectangular scaffolds; (b) stress–strain response under tensile loading of the multi-stiffness scaffolds; (c) and (d) tensile loading of the scaffolds revealed their spatially variable mechanical properties, with the 30% DM PGS-M region experiencing the greatest strain and the 80% DM region the least; (e) SEM of the interiors of the multi-stiffness scaffolds showed good integration between the different PGS-M regions. No discontinuities were clear at the boundaries between the 30 and 50% DM PGS-M regions (left arrow) or the 50 and 80% DM PGS-M regions (right arrow). Scale bars are 5 mm for (a), (c) and (d), and 1 mm for (e).

Tissue engineering scaffolds with spatially variable mechanical properties have previously been generated using electrospinning.[69] These scaffolds combined polymers with different mechanical properties at a varying ratio during the electrospinning process. The stiffness of the resulting scaffolds varied along their length from ~2 up to ~16 MPa. The applications of these scaffolds are limited however, due to the geometries that can be produced when using electrospinning. Multi-material 3D printing has also been used to produce tissue engineering scaffolds with regions of different stiffness; however, the pore sizes achievable were considerably larger than those possible through using porogen leaching (>500 μm).[70]

This simple proof-of-concept triphasic scaffold design demonstrates how a porous scaffold with spatially variable mechanical properties can be easily constructed using PGS-M combined with porogen leaching. This approach may have applications in engineering tissues where transitions between regions of different mechanical properties are present, such as cartilage,[52] ligaments and tendons.[53] Scaffold stiffness has been shown to affect cell function and fate in tissue engineering, and thus the ability to spatially vary scaffold mechanical properties produces valuable additional tuning options.[27]

Subtractive manufacturing of porous PGS-M scaffolds

PGS-M was combined with sucrose particles and photocured to produce a composite structure which was then processed using traditional, subtractive, manufacturing methods to generate macroscopic scaffold geometries. Subsequent leaching of the sucrose porogens from the machined scaffolds produced the microscopic scaffold porosity.

A molar crown and an orbital floor plate were produced as proof-of-concept scaffold designs (Figure 6). The PGS-M and sucrose composite demonstrated excellent machining characteristics. No cracking or chipping of the composite occurred as a result of the machining process. The CNC milling machine produced highly accurate scaffold geometries. Post machining, features of the orbital floor plate measured within a tolerance of ±0.06 mm compared to the CAD models they were produced from. However, some shrinkage of the scaffolds occurred following leaching of the sucrose porogens and freeze-drying, as had been observed previously in the disk-shaped scaffolds. The pore structure of the scaffolds appeared similar to that of the disk-shaped and tubular scaffolds produced using the same ratio of PGS-M to sucrose particles.

Utilising subtractive manufacturing techniques, via CNC machining, to process the macroscopic geometry of microporous scaffold materials has been described previously in bone tissue engineering for craniofacial applications. Porous hydroxyapatite scaffolds and decellularised bovine trabecular bone have been processed using CNC milling to produce custom implants for temporomandibular joint condyle repair.[71,72] Custom implants for alveolar ridge, maxillary ridge and maxillary sinus augmentation have also been produced using CNC machining of microporous biphasic calcium-phosphate and hydroxyapatite scaffolds.[73–75] Additionally, CNC machining has been successfully used to add perfusion channels to bone tissue-engineering scaffolds to improve nutrient/waste transport and promote cell infiltration.[76] To our knowledge, this is the first report of utilising digital design methods and CNC machining combined with porogen leaching to generate intricate porous scaffolds composed of a degradable elastomeric biomaterial.

The combination of subtractive manufacturing and porogen leaching enables the production of bespoke and highly detailed microporous scaffold designs using established technology. This may be particularly advantageous in applying this technology in a clinical solution, allowing for accelerated adoption due to the use of ubiquitous equipment. With the included sucrose particles acting as mechanical support, scaffolds may be machined from composites containing more elastic variants of PGS-M than the 80% DM polymer demonstrated herein. This offers the potential for a range of applications in both hard and soft tissue engineering, exploiting the ability to tune the mechanical properties and degradation rate of PGS-M.[26]

Additive manufacturing of porous PGS-M scaffolds

A hybrid process combining additive manufacturing and porogen leaching was developed for the fabrication of porous PGS-M scaffolds with highly versatile, user-defined, geometries. This process employed the selective photocuring of thin layers of compacted PGS-M and sucrose mixture to build up a 3D structure. As a proof-of-concept, a porous structure composed of a simple spiral of disks was produced (Figure 7). Following the selective photocuring process, methanol washing removed the unreacted, soluble, PGS-M prepolymer and surrounding sucrose particles, revealing the layered, photocured, structure with included sucrose particles (see Supplemental video). The construct conformed to the intended design. However, the diameter of the spiralling disks (~12 mm) appeared to exceed the diameter of the aperture through which they were photocured (8 mm). This was likely a result of scattering of the incident UV light by the PGS-M and sucrose mixture. Dissolving the included sucrose particles produced a

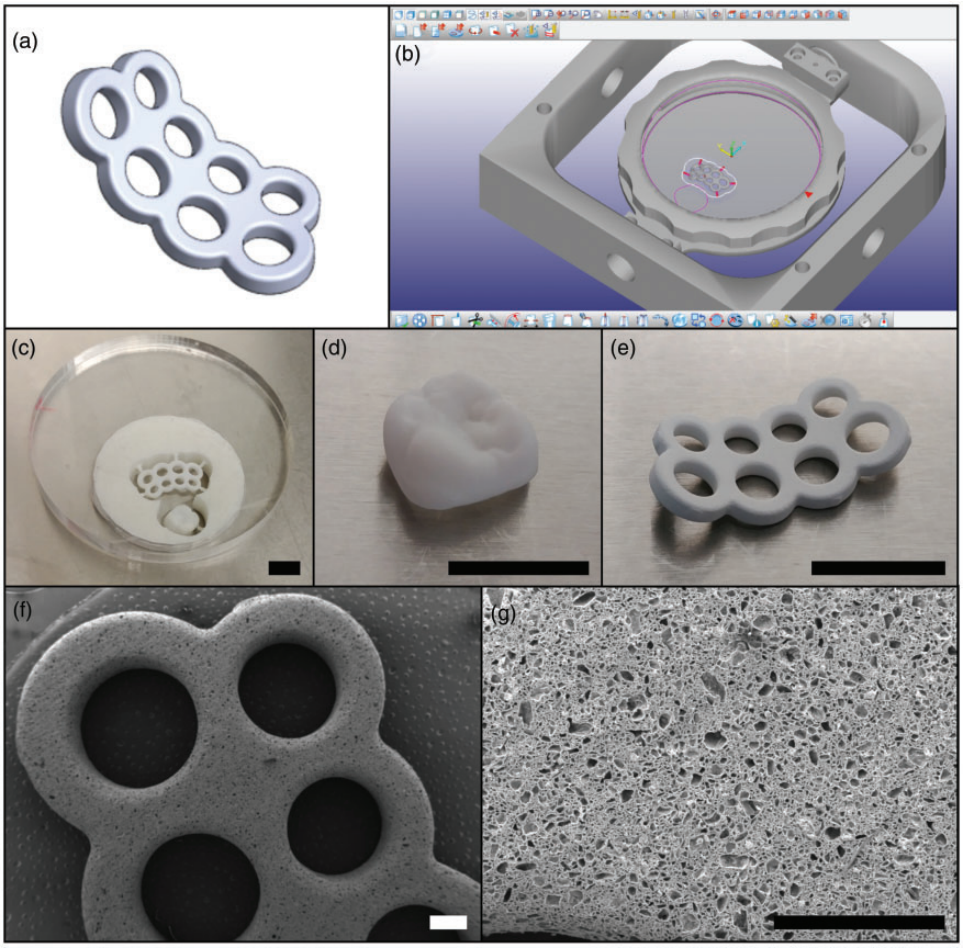

Figure 6. Subtractive manufacturing of porous PGS-M scaffolds: (a) the scaffolds were designed digitally, using CAD software, and then processed using CAM software (b) to generate the cutting path for the CNC machining process; (c) the scaffold designs were machined from a 10 mm thick disk of photocured PGS-M with included sucrose particles. A molar crown (d) and an orbital floor plate (e) were produced to demonstrate the capabilities of the process; (f) and (g) following sucrose leaching, SEM of the orbital floor plate showed excellent manufacturing quality and a highly porous structure. Scale bars for (c)–(e) are 10 mm and for (f) and (g) are 1 mm.

porous structure with similar handling properties to the disk-shaped and tubular PGS-M scaffolds. SEM revealed the scaffold surface and interior was porous. No discernible discontinuity was visible between the sequentially photocured layers of PGS-M, suggesting the scaffold remained porous and interconnected across the layer boundaries.

Combining additive manufacturing processes and porogen leaching has seen only limited exploration as a method for generating porous scaffolds for tissue engineering. A simple, but labour intensive, approach has been described, based on laminating layers of scaffold material together, after leaching of the porogen particles, to build up a 3D structure.[77] In bone tissue engineering, macroporous and microporous scaffolds were produced from hydroxyapatite combined with polyethylene porogens using robocasting, an extrusion-based additive manufacturing method.[78,79] This technique was used to produce patient-matched scaffold geometries for mandibular reconstruction. More recently, an extrusion-based 3D-printing method was used to produce scaffold structures from layered filaments of PGS mixed with included NaCl porogens.[80] The porogen particles provided mechanical support, preventing structural collapse during the extrusion and subsequent thermal curing process. Porogen removal by solvent washing then generated microporosity within the printed scaffolds. Although a number of intricate geometries were demonstrated, the height of these scaffolds appeared limited to only a few millimetres, and their porosity could not exceed $61.3 \pm 6.6\%$ due to difficulties in extruding filaments with greater porogen contents. The applications for these scaffolds in tissue engineering may therefore be restricted. Alternatively to porogen leaching, other methods have been coupled with additive manufacturing to generate microporosity in

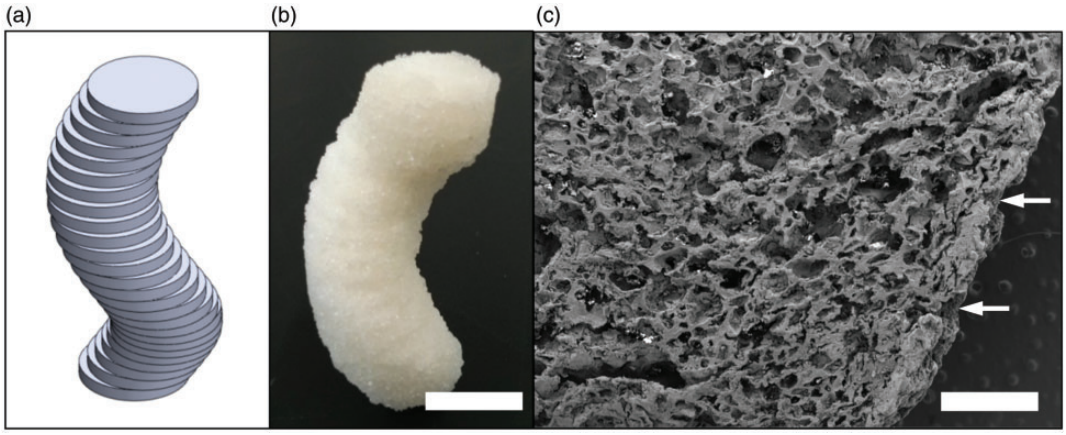

Figure 7. Additive manufacturing of porous PGS-M scaffolds: (a) digital scaffold design concept; (b) scaffold produced by selective photocuring of layers of PGS-M mixed with sucrose particles; (c) SEM following sucrose leaching showed the scaffold interiors were porous. No clear boundaries were visible between the sequentially photocured layers of PGS-M (arrows). Scale bars for (b) and (c) are 10 mm and 1 mm, respectively.

macroscopically defined structures, such as phase separation[81] and emulsion templating.[82]

The hybrid method presented here utilised the versatile additive manufacturing process to define the macrogeometry of the scaffold and the porogen leaching process to generate the microgeometry of the pores. Although digitally defining scaffold pore architectures is possible, recreating these at the scale required for tissue engineering applications through the use of additive processes alone is challenging. This is due to the labour-intensive methods required to accurately produce feature sizes in the tens of microns, such as 2PP.[26]

A promising proof-of-concept is presented here, utilising additive manufacturing combined with porogen leaching to produce porous PGS-M scaffolds. In future developments, it would be desirable to enhance the selective photocuring mechanism by using image projection to define the geometry of each PGS-M and sucrose layer. This, coupled to an automated method of delivering each additional layer of PGS-M and sucrose mixture into the build chamber, will produce a system capable of rapidly generating a wide range of digitally defined scaffold geometries. This process offers the potential to produce more versatile scaffold geometries than the mould-based or subtractive manufacturing methods for scaffold fabrication alternatively presented herein.

Conclusions

PGS-M is a highly versatile biomaterial with the favourable characteristics of PGS, including high elasticity and rapid degradation under physiological conditions, plus improved processing capabilities and tuneable mechanical properties. Here, various methods are presented for producing porous tissue engineering scaffolds from PGS-M in combination with sucrose porogens. These methods capitalised on the ability to rapidly crosslink PGS-M, imparted by its photocurable nature, allowing a more diverse and intricate range of scaffold designs to be realised compared to those achievable through using conventional, thermally cured, PGS.

A key advantage of the hybrid manufacturing methods that have been developed is the ability to tailor the macroscopic and microscopic features of the scaffolds separately. The macroscopic geometry of the scaffolds may be defined using simple moulds or cutting dies or through digital design methods linked to subtractive or additive manufacturing processes. The microscopic geometry of the scaffolds can be controlled by the selection the porogen particles which may vary in size, shape and material and alter the pore structure of the resulting scaffolds. Additionally, the combination of PGS-M with porogen leaching also permitted the production of porous scaffolds with spatially variable mechanical properties. This offers another level of flexibility in the design of tissue engineering scaffolds made from this tunable and degradable polymer and opens interesting avenues in the engineering of spatially anisotropic tissue, such as bone-muscle and bone-cartilage junctions.

The techniques presented here serve as examples of the potential of PGS-M combined with porogen leaching as a simple and powerful approach for producing tissue engineering scaffolds suitable for a wide range of applications. These hybrid manufacturing strategies are also highly flexible, offering the capabilities to be utilised together, in various combinations. For example, additive and subtractive manufacturing could be coupled together allowing for precise post-processing

operations following 3D printing. Alternatively, combining PGS-M polymers of different stiffness together during additive manufacturing may allow for the production of highly complex porous scaffolds with spatially resolved mechanical and structural properties.

A foundation is now established from which to develop further research. Additionally, with the possibility of transferring these manufacturing techniques to other photocurable polymers and alternative porogen materials, their utility could be expanded even further. There is even the potential to employ the technology beyond the field of tissue engineering, such as in sensors, soft actuators and catalyst supports where the lightweight and high surface area of the porous structures that may be fabricated would be considered as highly attractive properties.[83–87]

Acknowledgements

The authors would like to thank Jonathan Field for his assistance with the SEM images.

Declaration of conflicting interests

The author(s) declared no potential conflicts of interest with respect to the research, authorship, and/or publication of this article.

Funding

The author(s) disclosed receipt of the following financial support for the research, authorship, and/or publication of this article: This study was supported by the Engineering and Physical Sciences Research Council (Award 1624504 and Doctoral Prize Fellowship).

ORCID iD

Samand Pashneh-Tala https://orcid.org/0000-0003-2109-5494

Supplemental material

Supplemental material for this article is available online.

References

1. Khademhosseini A and Langer R. A decade of progress in tissue engineering. *Nat Protoc* 2016; 11: 1775–1781.
2. Jafari M, Paknejad Z, Rad MR, et al. Polymeric scaffolds in tissue engineering: a literature review: polymeric scaffolds in tissue engineering. *J Biomed Mater Res Part B Appl Biomater* 2017; 105: 431–459.
3. Rai R, Tallawi M, Grigore A, et al. Synthesis, properties and biomedical applications of poly(glycerol sebacate) (PGS): a review. *Prog Polym Sci* 2012; 37: 1051–1078.
4. Kharaziha M, Nikkhah M, Shin S-R, et al. PGS:gelatin nanofibrous scaffolds with tunable mechanical and structural properties for engineering cardiac tissues. *Biomaterials* 2013; 34: 6355–6366.
5. Chen Q-Z, Ishii H, Thouas GA, et al. An elastomeric patch derived from poly(glycerol sebacate) for delivery of embryonic stem cells to the heart. *Biomaterials* 2010; 31: 3885–3893.
6. Radisic M, Park H, Martens TP, et al. Pre-treatment of synthetic elastomeric scaffolds by cardiac fibroblasts improves engineered heart tissue. *J Biomed Mater Res A* 2008; 86: 713–724.
7. Lee K-W, Gade PS, Dong L, et al. A biodegradable synthetic graft for small arteries matches the performance of autologous vein in rat carotid arteries. *Biomaterials* 2018; 181: 67–80.
8. Wu W, Allen RA and Wang Y. Fast-degrading elastomer enables rapid remodeling of a cell-free synthetic graft into a neoartery. *Nat Med* 2012; 18: 1148–1153.
9. Lee K-W, Stolz DB and Wang Y. Substantial expression of mature elastin in arterial constructs. *Proc Natl Acad Sci USA* 2011; 108: 2705–2710.
10. Pritchard CD, Arnér KM, Langer RS, et al. Retinal transplantation using surface modified poly(glycerol-*co*-sebacic acid) membranes. *Biomaterials* 2010; 31: 7978–7984.
11. Sundback CA, Shyu JY, Wang Y, et al. Biocompatibility analysis of poly(glycerol sebacate) as a nerve guide material. *Biomaterials* 2005; 26: 5454–5464.
12. Hagandora CK, Gao J, Wang Y, et al. Poly (glycerol sebacate): a novel scaffold material for temporomandibular joint disc engineering. *Tissue Eng Part A* 2012; 19: 729–737.
13. Kemppainen JM and Hollister SJ. Tailoring the mechanical properties of 3D-designed poly(glycerol sebacate) scaffolds for cartilage applications. *J Biomed Mater Res A* 2010; 94: 9–18.
14. Jeong CG and Hollister SJ. A comparison of the influence of material on in vitro cartilage tissue engineering with PCL, PGS, and POC 3D scaffold architecture seeded with chondrocytes. *Biomaterials* 2010; 31: 4304–4312.
15. Wang Y, Ameer GA, Sheppard BJ, et al. A tough biodegradable elastomer. *Nat Biotechnol* 2002; 20: 602–606.
16. Li Y, Cook WD, Moorhoff C, et al. Synthesis, characterization and properties of biocompatible poly(glycerol sebacate) pre-polymer and gel. *Polym Int* 2013; 62: 534–547.
17. Lee M, Wu BM and Dunn J. Effect of scaffold architecture and pore size on smooth muscle cell growth. *J Biomed Mater Res A* 2008; 87: 1010–1016.
18. Karande TS, Ong JL and Agrawal CM. Diffusion in musculoskeletal tissue engineering scaffolds: design issues related to porosity, permeability, architecture, and nutrient mixing. *Ann Biomed Eng* 2004; 32: 1728–1743.
19. Zeltinger J, Sherwood JK, Graham DA, et al. Effect of pore size and void fraction on cellular adhesion, proliferation, and matrix deposition. *Tissue Eng* 2001; 7: 557–572.
20. Zhang R and Ma PX. Synthetic nano-fibrillar extracellular matrices with predesigned macroporous architectures. *J Biomed Mater Res* 2000; 52: 430–438.

21. Gomes ME, Rodrigues MT, Domingues RMA, et al. Tissue engineering and regenerative medicine: new trends and directions – a year in review. *Tissue Eng Part B Rev* 2017; 23: 211–224.
22. Wang M, Lei D, Liu Z, et al. A poly(glycerol sebacate) based photo/thermo dual curable biodegradable and biocompatible polymer for biomedical applications. *J Biomater Sci Polym Ed* 2017; 28: 1728–1739.
23. Bodakhe S, Verma S, Garkhal K, et al. Injectable photo-crosslinkable nanocomposite based on poly(glycerol sebacate) fumarate and hydroxyapatite: development, biocompatibility and bone regeneration in a rat calvarial bone defect model. *Nanomedicine (Lond)* 2013; 8: 1777–1795.
24. Ifkovits JL, Padera RF and Burdick JA. Biodegradable and radically polymerized elastomers with enhanced processing capabilities. *Biomed Mater* 2008; 3: 034104.
25. Nijst CLE, Bruggeman JP, Karp JM, et al. Synthesis and characterization of photocurable elastomers from poly(glycerol-*co*-sebacate). *Biomacromolecules* 2007; 8: 3067–3073.
26. Pashneh-Tala S, Owen R, Bahmaee H, et al. Synthesis, characterization and 3D micro-structuring via 2-photon polymerization of poly(glycerol sebacate)-methacrylate – an elastomeric degradable polymer. *Front Phys*. Epub ahead of print 8 May 2018. DOI: 10.3389/fphy.2018.00041.
27. Kumar A, Placone JK and Engler AJ. Understanding the extracellular forces that determine cell fate and maintenance. *Development* 2017; 144: 4261–4270.
28. Sridhar BV, Brock JL, Silver JS, et al. Development of a cellularly degradable PEG hydrogel to promote articular cartilage extracellular matrix deposition. *Adv Healthcare Mater* 2015; 4: 702–713.
29. O'Dea RD, Osborne JM, El Haj AJ, et al. The interplay between tissue growth and scaffold degradation in engineered tissue constructs. *J Math Biol* 2013; 67: 1199–1225.
30. Ghosh K and Ingber DE. Micromechanical control of cell and tissue development: implications for tissue engineering. *Adv Drug Deliv Rev* 2007; 59: 1306–1318.
31. Engler AJ, Sen S, Sweeney HL, et al. Matrix elasticity directs stem cell lineage specification. *Cell* 2006; 126: 677–689.
32. Thadavirul N, Pavasant P and Supaphol P. Development of polycaprolactone porous scaffolds by combining solvent casting, particulate leaching, and polymer leaching techniques for bone tissue engineering. *J Biomed Mater Res A* 2014; 102: 3379–3392.
33. Meinel L, Karageorgiou V, Hofmann S, et al. Engineering bone-like tissue in vitro using human bone marrow stem cells and silk scaffolds. *J Biomed Mater Res A* 2004; 71: 25–34.
34. Burdick JA, Frankel D, Dernell WS, et al. An initial investigation of photocurable three-dimensional lactic acid based scaffolds in a critical-sized cranial defect. *Biomaterials* 2003; 24: 1613–1620.
35. Baheiraei N, Yeganeh H, Ai J, et al. Preparation of a porous conductive scaffold from aniline pentamer-modified polyurethane/PCL blend for cardiac tissue engineering. *J Biomed Mater Res A* 2015; 103: 3179–3187.
36. Laschke MW, Strohe A, Menger MD, et al. In vitro and in vivo evaluation of a novel nanosize hydroxyapatite particles/poly(ester-urethane) composite scaffold for bone tissue engineering. *Acta Biomater* 2010; 6: 2020–2027.
37. Grenier S, Sandig M and Mequanint K. Polyurethane biomaterials for fabricating 3D porous scaffolds and supporting vascular cells. *J Biomed Mater Res A* 2007; 82: 802–809.
38. Falco EE, Wang MO, Thompson JA, et al. Porous EH and EH-PEG scaffolds as gene delivery vehicles to skeletal muscle. *Pharm Res* 2011; 28: 1306–1316.
39. Zhang J, Mujeeb A, Feng J, et al. Physically entrapped gelatin in polyethylene glycol scaffolds for three-dimensional chondrocyte culture. *J Bioact Compat Polym* 2016; 31: 513–530.
40. Zhang Q, Lu H, Kawazoe N, et al. Pore size effect of collagen scaffolds on cartilage regeneration. *Acta Biomater* 2014; 10: 2005–2013.
41. Pan Z, Duan P, Liu X, et al. Effect of porosities of bilayered porous scaffolds on spontaneous osteochondral repair in cartilage tissue engineering. *Regen Biomater* 2015; 2: 9–19.
42. Li C, Wang L, Yang Z, et al. A viscoelastic chitosan-modified three-dimensional porous poly(l-lactide-*co*-ε-caprolactone) scaffold for cartilage tissue engineering. *J Biomater Sci Polym Ed* 2012; 23: 405–424.
43. Aramwit P, Ratanavaraporn J, Ekgasit S, et al. A green salt-leaching technique to produce sericin/PVA/glycerin scaffolds with distinguished characteristics for wound-dressing applications. *J Biomed Mater Res Part B Appl Biomater* 2015; 103: 915–924.
44. Liang X, Qi Y, Pan Z, et al. Design and preparation of quasi-spherical salt particles as water-soluble porogens to fabricate hydrophobic porous scaffolds for tissue engineering and tissue regeneration. *Mater Chem Front* 2018; 2: 1539–1553.
45. Lin-Gibson S, Cooper JA, Landis FA, et al. Systematic investigation of porogen size and content on scaffold morphometric parameters and properties. *Biomacromolecules* 2007; 8: 1511–1518.
46. Huri PY, Ozilgen BA, Hutton DL, et al. Scaffold pore size modulates in vitro osteogenesis of human adipose-derived stem/stromal cells. *Biomed Mater* 2014; 9: 045003.
47. Matsiko A, Gleeson JP and O'Brien FJ. Scaffold mean pore size influences mesenchymal stem cell chondrogenic differentiation and matrix deposition. *Tissue Eng Part A* 2014; 21: 486–497.
48. Taherkhani S and Moztarzadeh F. Fabrication of a poly (ε-caprolactone)/starch nanocomposite scaffold with a solvent-casting/salt-leaching technique for bone tissue engineering applications. *J Appl Polym Sci*. Epub ahead of print 29 February 2016. DOI: 10.1002/app.43523.
49. Janik H and Marzec M. A review: fabrication of porous polyurethane scaffolds. *Mater Sci Eng C Mater Biol Appl* 2015; 48: 586–591.

50. Boffito M, Sartori S and Ciardelli G. Polymeric scaffolds for cardiac tissue engineering: requirements and fabrication technologies. *Polym Int* 2014; 63: 2–11.
51. Crapo PM, Gao J and Wang Y. Seamless tubular poly (glycerol sebacate) scaffolds: high-yield fabrication and potential applications. *J Biomed Mater Res A* 2008; 86: 354–363.
52. Yousefi A-M, Hoque ME, Prasad R, et al. Current strategies in multiphasic scaffold design for osteochondral tissue engineering: a review. *J Biomed Mater Res A* 2015; 103: 2460–2481.
53. Verdiyeva G, Koshy K, Glibbery N, et al. Tendon reconstruction with tissue engineering approach – a review. *J Biomed Nanotechnol* 2015; 11: 1495–1523.
54. Carnachan RJ, Bokhari M, Przyborski SA, et al. Tailoring the morphology of emulsion-templated porous polymers. *Soft Matter* 2006; 2: 608.
55. Sharifpoor S, Simmons CA, Labow RS, et al. Functional characterization of human coronary artery smooth muscle cells under cyclic mechanical strain in a degradable polyurethane scaffold. *Biomaterials* 2011; 32: 4816–4829.
56. Song Y, Wennink JWH, Kamphuis MMJ, et al. Dynamic culturing of smooth muscle cells in tubular poly(trimethylene carbonate) scaffolds for vascular tissue engineering. *Tissue Eng Part A* 2011; 17: 381–387.
57. Smith E and Dent G. Chapter 1 – introduction, basic theory and principles. In: *Modern Raman spectroscopy – a practical approach*. Hoboken, NJ: Wiley, 2005, pp.2–20.
58. Castor CA Jr, Pontier A, Durand J, et al. Real time monitoring of the quiescent suspension polymerization of methyl methacrylate in microreactors – part 1: a kinetic study by Raman spectroscopy and evolution of droplet size. *Chem Eng Sci* 2015; 131: 340–352.
59. Alberts B, Johnson A, Lewis J, et al. Chapter 1 – cells and genomes. In: *Molecular biology of the cell*. NY, USA: Garland Science, 2002, pp.1–45.
60. Gao J, Crapo PM and Wang Y. Macroporous elastomeric scaffolds with extensive micropores for soft tissue engineering. *Tissue Eng* 2006; 12: 917–925.
61. Oh SH, Kang SG, Kim ES, et al. Fabrication and characterization of hydrophilic poly(lactic-*co*-glycolic acid)/poly(vinyl alcohol) blend cell scaffolds by melt-molding particulate-leaching method. *Biomaterials* 2003; 24: 4011–4021.
62. Kim HD and Valentini RF. Retention and activity of BMP-2 in hyaluronic acid-based scaffolds in vitro. *J Biomed Mater Res* 2002; 59: 573–584.
63. Crapo PM and Wang Y. Physiologic compliance in engineered small-diameter arterial constructs based on an elastomeric substrate. *Biomaterials* 2010; 31: 1626–1635.
64. Gao J, Ensley AE, Nerem RM, et al. Poly(glycerol sebacate) supports the proliferation and phenotypic protein expression of primary baboon vascular cells. *J Biomed Mater Res A* 2007; 83: 1070–1075.
65. Pashneh-Tala S, MacNeil S and Claeyssens F. The tissue-engineered vascular graft – past, present, and future. *Tissue Eng Part B Rev* 2015; 22: 68–100.
66. Chian KS, Leong MF and Kono K. Regenerative medicine for oesophageal reconstruction after cancer treatment. *Lancet Oncol* 2015; 16: e84–e92.
67. Law JX, Liau LL, Aminuddin BS, et al. Tissue-engineered trachea: a review. *Int J Pediatr Otorhinolaryngol* 2016; 91: 55–63.
68. Scaffaro R, Lopresti F, Botta L, et al. Melt processed PCL/PEG scaffold with discrete pore size gradient for selective cellular infiltration. *Macromol Mater Eng* 2016; 301: 182–190.
69. Kishan AP, Robbins AB, Mohiuddin SF, et al. Fabrication of macromolecular gradients in aligned fiber scaffolds using a combination of in-line blending and air-gap electrospinning. *Acta Biomater* 2017; 56: 118–128.
70. Diaz-Gomez L, Smith BT, Kontoyiannis PD, et al. Multimaterial segmented fiber printing for gradient tissue engineering. *Tissue Eng Part C Methods* 2018; 25: 12–24.
71. Ciocca L, Donati D, Ragazzini S, et al. Mesenchymal stem cells and platelet gel improve bone deposition within CAD-CAM custom-made ceramic HA scaffolds for condyle substitution. *BioMed Res Int* 2013; Article Id: 549742.
72. Grayson WL, Fröhlich M, Yeager K, et al. Engineering anatomically shaped human bone grafts. *Proc Natl Acad Sci USA* 2010; 107: 3299–3304.
73. Luongo F, Mangano FG, Macchi A, et al. Custom-made synthetic scaffolds for bone reconstruction: a retrospective, multicenter clinical study on 15 patients. *BioMed Res Int. Epub ahead of print* 2016; 3: 1–12.
74. Mangano F, Macchi A, Shibli JA, et al. Maxillary ridge augmentation with custom-made CAD/CAM scaffolds. A 1-year prospective study on 10 patients. *J Oral Implantol* 2013; 40: 561–569.
75. Mangano F, Zecca P, Pozzi-Taubert S, et al. Maxillary sinus augmentation using computer-aided design/computer-aided manufacturing (CAD/CAM) technology. *Int J Med Robot* 2013; 9: 331–338.
76. Buckley CT and O'Kelly KU. Fabrication and characterization of a porous multidomain hydroxyapatite scaffold for bone tissue engineering investigations. *J Biomed Mater Res Part B Appl Biomater* 2010; 93: 459–467.
77. Lu L and Mikos AG. The importance of new processing techniques in tissue engineering. *MRS Bull* 1996; 21: 28–32.
78. Cesarano J, Dellinger JG, Saavedra MP, et al. Customization of load-bearing hydroxyapatite lattice scaffolds. *Int J Appl Ceram Technol*. 2005; 2: 212–220.
79. Tuttle BA, Smay JE, Cesarano J, et al. Robocast Pb $(Zr_{0.95}Ti_{0.05})O_3$ ceramic monoliths and composites. *J Am Ceram Soc* 2001; 84: 872–874.
80. Lei D, Yang Y, Liu Z, et al. A general strategy of 3D printing thermosets for diverse applications. *Mater Horiz* 2019; 6: 394–404.
81. Li J, Zhang L, Lv S, et al. Fabrication of individual scaffolds based on a patient-specific alveolar bone defect model. *J Biotechnol* 2011; 151: 87–93.

82. Owen R, Sherborne C, Paterson T, et al. Emulsion templated scaffolds with tunable mechanical properties for bone tissue engineering. *J Mech Behav Biomed Mater* 2016; 54: 159–172.
83. Polygerinos P, Correll N, Morin SA, et al. Soft robotics: review of fluid-driven intrinsically soft devices; manufacturing, sensing, control, and applications in human-robot interaction. *Adv Eng Mater* 2017; 19: 1700016.
84. Feiner R, Engel L, Fleischer S, et al. Engineered hybrid cardiac patches with multifunctional electronics for online monitoring and regulation of tissue function. *Nat Mater* 2016; 15: 679–685.
85. Zhao Q, Dunlop JWC, Qiu X, et al. An instant multi-responsive porous polymer actuator driven by solvent molecule sorption. *Nat Commun* 2014; 5: 4293.
86. Bahramzadeh Y and Shahinpoor M. A review of ionic polymeric soft actuators and sensors. *Soft Robot* 2013; 1: 38–52.
87. Yang Y, Chiang K and Burke N. Porous carbon-supported catalysts for energy and environmental applications: a short review. *Catal Today* 2011; 178: 197–205.